Genesis of high-Ni olivine phenocrysts of the Dali picrites in the Central Emeishan large igneous province

Wen-Chang Cai[1] , Zhao-Chong Zhang[1], Jiang Zhu[1,2], M. Santosh[1,3] and Rong-Hao Pan[1]

[1]State Key Laboratory of Geological Processes and Mineral Resources, China University of Geosciences, Beijing, 100083, China; [2]Yunnan Institute of Geological Sciences, Kunming, 650051, China and [3]Department of Earth Sciences, University of Adelaide, Adelaide, SA 5005, Australia

Abstract

The Emeishan large igneous province (ELIP) in SW China is considered to be a typical mantle-plume-derived LIP. The picrites formed at relatively high temperatures in the ELIP, providing one of the important lines of argument for the role of mantle plume. Here we report trace-element data on olivine phenocrysts in the Dali picrites from the ELIP. The olivines are Ni-rich, and characterized by high (>1.4) $100 \times Mn/Fe$ value and low (<13) $10\,000 \times Zn/Fe$ value, indicating a peridotite-dominated source. Since the olivine–melt Ni partition coefficient ($K_D Ni^{ol/melt}$) will decrease at high temperatures and pressures, the picrites derived from peridotite melting at high pressure, and that crystallized olivines at lower pressure, can generate high concentrations of Ni in olivine phenocrysts, excluding the necessity of a metasomatic pyroxenite contribution. Based on the Al-in-olivine thermometer, olivine crystallization temperature and mantle potential temperature (T_P) were calculated at *c.* 1491°C and *c.* 1559°C, respectively. Our results are *c.* 200°C higher than that of the normal asthenospheric mantle, and are consistent with the role of a mantle thermal plume for the ELIP.

CAMBRIDGE
UNIVERSITY PRESS

1. Introduction

Large igneous provinces (LIPs) are characterized by voluminous volcanic sequences ($>10^5$ km^2; $>10^5$ km^3) erupting over a short period of time (1–5 Ma), and their formation is generally related to mantle plumes (Richards *et al.* 1989; Campbell & Griffins, 1990; Chung & Jahn, 1995; Campbell, 2005). The association of picrites with LIPs provide one of the important lines of evidence in favour of a relatively high-temperature plume source (He *et al.* 2003; Hanski *et al.* 2004; Ali *et al.* 2005; Campbell, 2005, 2007; Zhang *et al.* 2006; Shellnutt, 2014; Santosh *et al.* 2018; Condie & Puetz, 2019). However, some recent studies suggested that the source of the Emeishan large igneous province (ELIP) picrites involved variable proportions of pyroxenite or eclogites (Kamenetsky *et al.* 2012; Yu *et al.* 2014, 2017; Liu *et al.* 2017; Zhu *et al.* 2018). The presence of eclogites or pyroxenite in the mantle source region can lead to overestimates in temperature as the thermometers assume a peridotite-dominated source (e.g. olivine–liquid equilibrium for primary magmas produced by melting of fertile peridotite; Zhang *et al.* 2006; Herzberg, 2011; Shellnutt & Pham, 2018). One of the important challenges is therefore to clarify whether the mantle source of ELIP picrite is dominated by peridotite or pyroxenite.

As one of the earliest crystallized minerals from typical mantle-derived magmas, the composition of olivine phenocrysts with high Fo values (atomic $100 \times Mg/(Mg + Fe)$) can provide important information on the primary magma. Recent studies suggest that some trace elements (such as Mn and Zn) in olivine from pyroxenite-derived and peridotite-derived melts have two distinct trends (Le Roux *et al.* 2010; Howarth & Harris, 2017) and can therefore be used to distinguish pyroxenite components in the mantle source region. Some studies recorded picritic rocks in the inner zone of the ELIP (Hanski *et al.* 2010; Kamenetsky *et al.* 2012; Yu *et al.* 2017; Yao *et al.* 2019), which were thought to have formed at relatively high temperatures (Xu *et al.* 2001; Zhang *et al.* 2004, 2006; Shellnutt & Pham, 2018). However, some other studies suggested that the picrites were derived from a metasomatized pyroxenite-bearing mantle source (Kamenetsky *et al.* 2012; Yu *et al.* 2017). The role of high-temperature primary magmas in the ELIP therefore remains contentious. In this paper, we investigate this aspect based on petrology and mineral chemistry of olivine phenocrysts from Dali picrite in the inner zone of the ELIP, with a view to evaluate the nature of the mantle source and the conditions of melting.
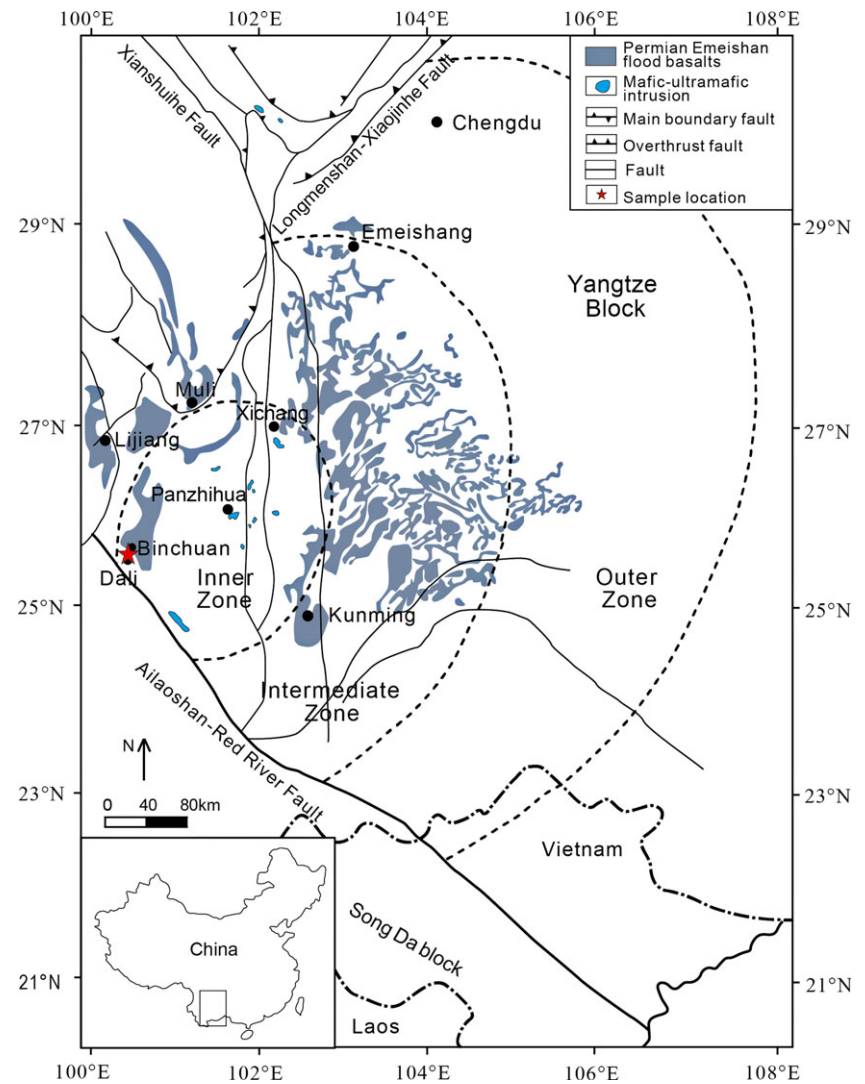
Fig. 1. (Colour online) Simplified regional geological map of the Emeishan large igneous province showing the concentric zones (dashed grey line), volcanic and intrusive rocks, and sampling location (modified after Kamenetsky *et al.* 2012; Wu *et al.* 2018).

2. Geological setting

The ELIP is mainly located in the western part of the Yangtze craton in SW China (Fig. 1). Its southwestern margin is bounded by the Ailaoshan–Red River Fault, and the northwestern boundary is traditionally thought to be the Longmenshan–Xiaojinhe Fault. The volcanic successions in the ELIP trend N–S with a rhombic shape and cover an area of more than 2.5×10^5 km², with a total erupted volume of more than 3×10^5 km³ (Xu *et al.* 2001, 2004; Ali *et al.* 2005, 2010). The thickness of the volcanic sequence ranges from *c.* 5000 m to several hundred metres, with the thickest zone located near the Lijiang and Binchuan sections in the western part of the ELIP and the thinnest area located in the eastern part of the ELIP (Xu *et al.* 2004; Song *et al.* 2001, 2004; Xiao *et al.* 2003, 2004; Zhang *et al.* 2006). The ELIP comprises a succession of tholeiites, with minor picritic and rhyolitic/trachytic lava flows. Many mafic-ultramafic intrusions are exposed in a belt extending along the Panzhihua–Xichang region in the SW part of the ELIP, and some of these intrusions host giant Fe-Ti-V oxide and Ni-Cu-PGE sulphide deposits (Shellnutt, 2014). Previous studies have indicated that the main phase of magmatism took place at *c.* 260 Ma over a short duration of 1 Ma (Zhou *et al.* 2002; He *et al.* 2007; Shellnutt *et al.* 2008, 2012; Zhong *et al.* 2009, 2011, 2014; Sun *et al.* 2010; Xu *et al.* 2010; Jerram *et al.* 2016).

The picritic lavas mainly occur in the central ELIP such as those in the Dali and Binchuan districts, and these areas are considered to represent the centre of the mantle plume (Zhang *et al.* 2006; Hanski *et al.* 2010; Kamenetsky *et al.* 2012; Li *et al.* 2015; Ren *et al.* 2017; Wu *et al.* 2018). The samples of Dali picrite for this study were collected from a road-cut section *c.* 20 km NE of Dali City (25° 40′ 48″ N; 100° 21′ 14″ E), the occurrence of which was reported by Hanski *et al.* (2010) and Ren *et al.* (2017). The picrites occur in the bottom part of the Emeishan basaltic sequence (Fig. 2a). A newly opened quarry from where the basalts and picrites are mined exposes fresh outcrops, where the picrites are easily distinguished from their darker colour compared with the associated basalt flows.

Most of the picrites are porphyritic (with 20–40 vol% phenocrysts), and the dominant phenocryst is olivine (*c.* 80 vol% of the phenocrysts) with minor clinopyroxene. The olivine phenocrysts are subhedral to euhedral, generally ranging from 0.2 to 2 mm across with the largest grains up to 4 mm in diameter. Some olivine crystals are altered to serpentine along the rims and cracks, but their cores remain unaltered. Minor euhedral to subhedral Cr-spinel grains occur within the olivine phenocrysts (Fig. 2c). The groundmass consists predominantly of microcrystalline–cryptocrystalline olivine, anhedral clinopyroxene and small
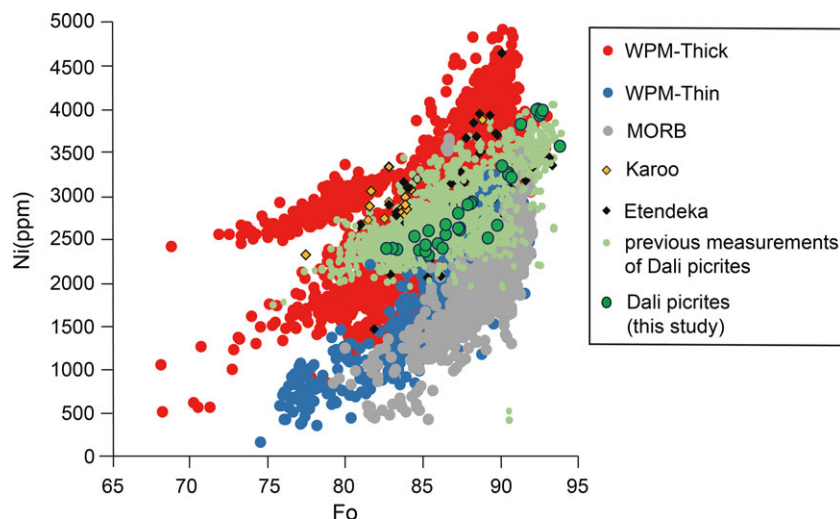
Fig. 3. (Colour online) Relationship between the forsterite (Fo) content and Ni concentration in olivine from picrites erupted on thick and thin lithosphere. Dali picrite data were analysed by LA-ICP-MS; errors on measurements are smaller than the symbols. WPM-thick and WPM-thin data from Sobolev *et al.* (2007). Karoo and Etendeka data from Howarth & Harris (2017). The previously measured olivine Dali picrite data are from Hanski *et al.* (2010) and Yu *et al.* (2017). WPM – within-plate magmas.

plagioclase crystals. Some Cr-spinels and Fe-Ti oxide minerals occur in the groundmass.

The basalts are porphyritic (with 15–40 vol% phenocrysts), and plagioclase is the dominant phenocryst (*c.* 80–90 vol% of the phenocrysts; Fig. 2d) with minor clinopyroxene (*c.* 10–20 vol% of the phenocrysts). The groundmass consists predominantly of microcrystalline plagioclase, anhedral clinopyroxene, some basaltic glass and a small amount of magnetite and Fe-Ti oxide.

3. Analytical methods

Polished thin-sections of picrite samples were prepared for the analysis. The olivine phenocrysts selected for analysis show little alteration with no zoning. The unaltered Cr-spinel inclusions without any fractures were selected for analysis.

Major and minor elements in olivines and Cr-spinels were analysed using an EPMA-1720 electron microprobe at the EPMA Laboratory, Institute of Earth Sciences, China University of Geosciences, Beijing (CUGB). For most elements, the accelerating voltage was 15 kV, beam current 20 nA and beam diameter 1 μm, with the on-peak counting time set for 10 s per element and 5 s for background. The Al element was analysed using a 60 s peak counting time and the background was set for 30 s. The standard samples are natural minerals and synthetic oxides produced by SPI Supplies of the United States of America. The precision is better than 1% for most major and minor elements.

Trace-element concentrations of olivine were determined by laser ablation – inductively coupled plasma – mass spectrometry (LA-ICP-MS) using the Agilent 7900 Quadrupole ICP-MS coupled with a Photon Machines Analyte HE 193 nm ArF Excimer laser ablation system. The analyses were carried out at the Mineral Geochemistry Lab, Ore Deposit and Exploration Centre (ODEC), Hefei University of Technology, China. In this study, the ablation protocol employed a spot of 30 μm diameter at 8 Hz with an energy of *c.* 4 J cm^{-2} fluence. Each spot was measured for 40 s, and each spot analysis was followed by a gas blank for 20 s. Helium was used as the carrier gas and argon was used as the make-up gas, and they were mixed via a T-connector before entering the ICP (Ning *et al.* 2017; Wang *et al.* 2017). Reference materials GSE-1G, GSD-1G, BCR-2G and SRM-612 were used as external standards, and they were measured every 10–12 spot analyses to

check reproducibility through the analytical session. Off-line selection and the integration of background and analytical signals, and time-drift correction and quantitative calibration, were performed with ICP-MS Data Cal (Liu *et al.* 2008). The precision for most trace elements in each spot was better than 10%.

4. Mineral chemistry of olivine and Cr-spinel

The major elements and some minor elements (Ni, Mn and Al) were analysed by EPMA, and all the analytical spots were on fresh core regions of the grains (online Supplementary Table S1a, available at http://journals.cambridge.org/geo). The olivine phenocrysts show Fo values of 82.1–93.3. The grains with low Fo values (Fo < 85) are relatively small in size compared with those with high Fo values (Fo > 85). Most olivine grains with high Fo values show 0.2–0.4 mm diameter with a few cracks, whereas those grains with low Fo values are mainly 0.1–0.2 mm in diameter.

Generally, the content of NiO (0.25–0.51 wt%) shows a positive correlation with the Fo values, whereas the MnO content displays a negative correlation with the Fo values (0.11–0.32 wt%). The CaO concentration is relatively high, ranging from 0.25 to 0.46 wt%, with no correlation with the olivine Fo values. The Al$_2$O$_3$ content in olivine range from 0.03 to 0.11 wt%. All the olivine phenocrysts of the Dali picrites contain > 0.25 wt% CaO content, and exhibit no kinked band. We infer that they were crystallized from magma and are not mantle xenocrysts, and can therefore be used as an indicator of the primary melt.

With regard to the minor- and trace-element concentrations in the core of the olivine phenocrysts (analysed by LA-ICP-MS), the Ni concentration ranges from 2563 to 3897 ppm (0.32–0.49 wt% NiO) and shows a positive correlation with the Fo values (Fig. 3). The CaO concentration ranges from 0.25 to 0.50 wt%. MnO content ranges from 0.11 to 0.22 wt% (Fig. 4), whereas the Zn concentration range is 49.8–120.9 ppm, showing a positive Zn–Mn correlation (Fig. 5a; online Supplementary Table S2, available at http://journals.cambridge.org/geo). In addition, the olivine contains 115.6–171.1 ppm Co, 5.8–21.1 ppm V and 4.4–8.9 ppm Sc. However, most rare earth elements (REEs), especially light REEs (LREEs), are present in quantities lower than the detection limits. Although some minor elements such as Ni and Mn were analysed by both EPMA and LA-ICP-MS, we discuss the LA-ICP-MS data as it is of greater precision.
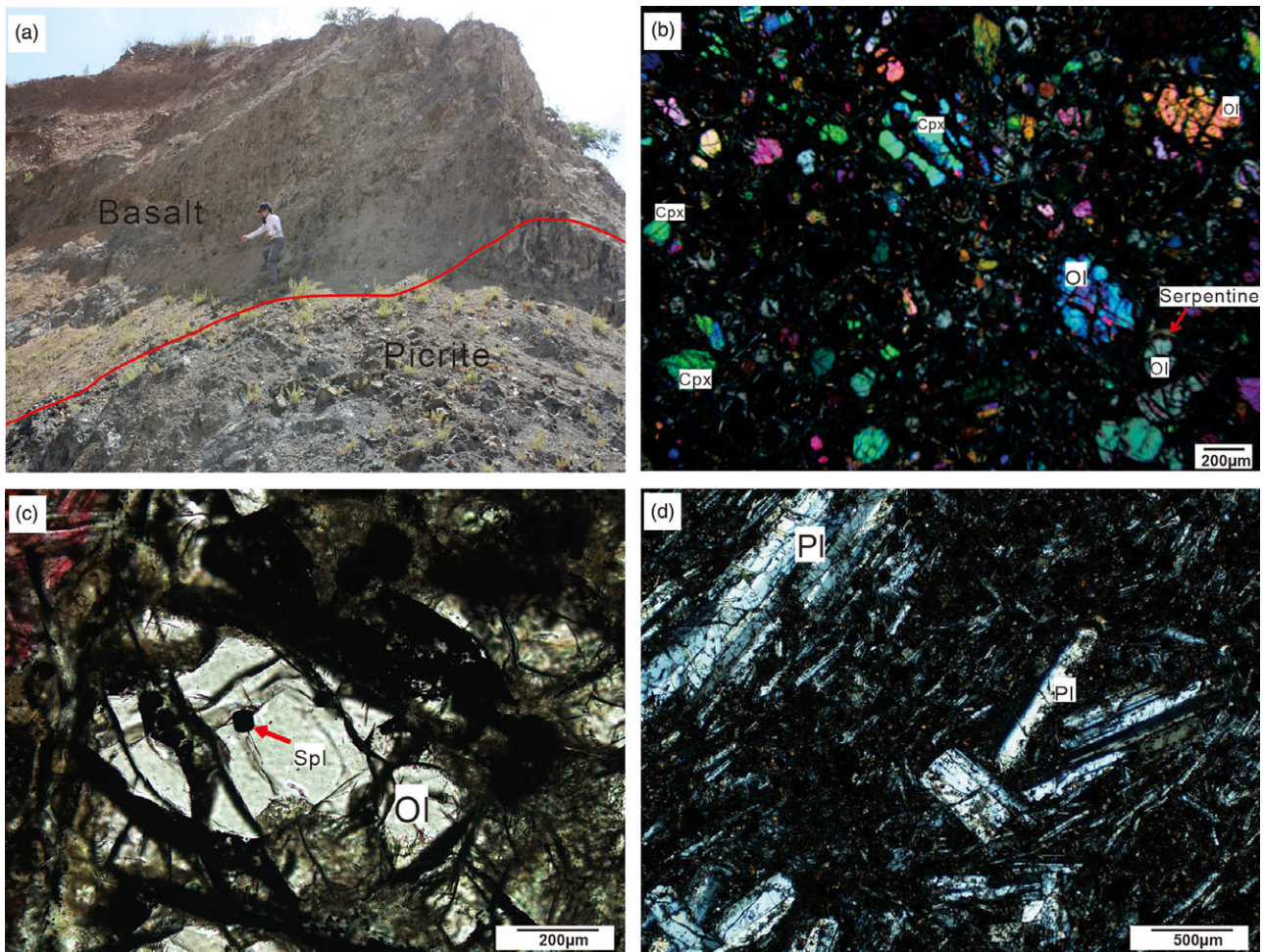
Fig. 2. (Colour online) (a) Picritic lava showing sharp contact with basalt in the Dali geological section. (b) Olivine and clinopyroxene phenocrysts in Dali picrite (cross-polarized light). (c) Small Cr-spinel grains included by olivine phenocryst (plane-polarized light). (d) Plagioclase phenocrysts in those basalts that coexist with Dali picrites (cross-polarized light).
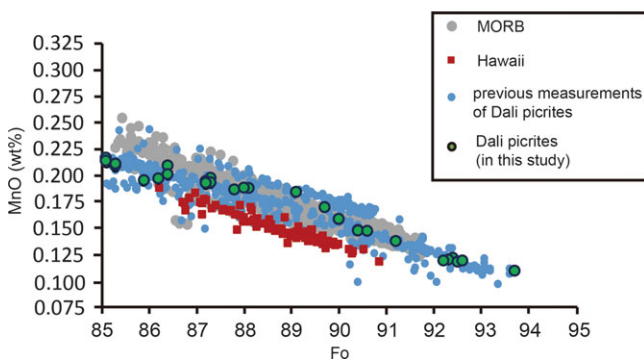

Fig. 4. (Colour online) The forsterite (Fo) values versus MnO concentrations in olivine phenocrysts. Dali picrite data analysed by LA-ICP-MS; errors on measurements are smaller than the symbols. Olivine MORB and Hawaii data from Sobolev *et al.* (2005, 2007) and the previously measured olivine Dali picrite data are from Hanski *et al.* (2010) and Yu *et al.* (2017).

The Cr no. (atomic Cr/(Cr + Al)) of Cr-spinel ranges from 0.570 to 0.685 (online Supplementary Table S1b). The content of TiO_2 is in the range of 0.4–1.8 wt%, and total iron as FeO (FeO*) is 19.5–29.2 wt%. The MgO contents vary from 9.7 to 14.3 wt%, and the Al_2O_3 values range from 16.4 to 20.8 wt%.

5. Discussion

5.a. Origin of high-Ni olivine

The Ni content of primitive mantle is estimated as 1960 ppm, which is similar to that of the depleted peridotite (McDonough & Sun, 1995; Herzberg *et al.* 2013), whereas the Ni concentration of olivine in mantle peridotite ranges from 2800 to 3100 ppm (Ionov, 2007; Herzberg *et al.* 2013, 2016). However, the olivine phenocrysts in Dali picrites, especially those grains with high Fo values, have much higher Ni concentration (with Ni concentration up to c. 3900 ppm, Hanski *et al.* 2010; Yu *et al.* 2017) than those from mid-ocean ridge basalts (MORBs) or mantle peridotite (Fig. 3). The excess Ni in olivine can result from the following processes. (1) The core–mantle interaction can produce a less-degassed Ni-rich source, and this source continues adding into the mantle plume, which finally formed picrites with high Ni content (Herzberg *et al.* 2013, 2016). (2) The silica-rich melts formed from recycled crust might interact with mantle peridotite to form a secondary olivine-poor pyroxenite source. Magmas derived from such metasomatic pyroxenite source would therefore contain higher Ni content than those derived from peridotite source (Sobolev *et al.* 2005, 2007; Herzberg, 2006; Foley *et al.* 2011, 2013). (3) Higher melting temperature and pressure would decrease the partition coefficient of Ni between olivine and melts ($K_D Ni^{ol/melt}$); this will

result in a higher Ni concentration in primary melt, and the olivine crystallizing from this melt will have higher Ni content (Niu *et al.* 2011; Putirka *et al.* 2011; Matzen *et al.* 2013, 2017).

Olivine with high Ni content has also been recognized in other LIPs. The picrites in Baffin Island and West Greenland also have olivine phenocrysts containing high Ni concentration (*c.* 3800 ppm) (Sobolev *et al.* 2007; Herzberg *et al.* 2013), even 20% higher than the modern MORB source (2800–3100 ppm) (Ionov, 2007). These picrites are characterized by elevated ^{3}He/^{4}He ratios (Starkey *et al.* 2009). Picrites from Baffin Island and West Greenland show ^{3}He/^{4}He values up to 50 times the atmospheric value. Herzberg *et al.* (2013) proposed that a less-degassed mantle reservoir formed by core–mantle interaction near the core–mantle boundary contains high ^{3}He/^{4}He, and they correlated the elevated ^{3}He/^{4}He associated with high Ni concentration to the less-degassed Ni-rich material from core–mantle boundary that was added to the mantle source region. For the ELIP, however, picrites from Dali, Binchuan and Lijiang area generally have higher Os concentration and slightly lower Re concentration than many other ocean island picrites, although the ^{187}Os/^{188}Os ratios are obviously lower than the mantle value with negative γOs values (Chen *et al.* 2007; Xu *et al.* 2007; Zhang *et al.* 2008; Li *et al.* 2010; Hao *et al.* 2011), which are distinctly different from the Siberia LIP picrites that display relatively positive γOs values. The Os isotopic compositions of the picrites in the ELIP therefore suggest no major input from the core–mantle boundary to the source region.

If the silica-rich melt derived from recycled crust reacts with peridotite, an olivine-free pyroxenite source can be generated that would produce magmas with high Ni concentration (Sobolev *et al.* 2005). Olivine crystallizing from such a magma will generally be characterized by high Ni concentration and low Mn/Fe. The Mn, Fe and Zn in olivine mostly occur as divalent elements and their ionic radii is close to that of Mg^{2+} (De Hoog *et al.* 2010); they therefore behave similarly in the olivine–melt system. Since Mn, Fe and Zn have similar olivine–melt partition coefficients (0.89, 1.1 and 1.09, respectively; Foley *et al.* 2013; Howarth & Harris, 2017), their ratios are relatively constant during partial melting or fractional crystallization. The ratios of these melts could therefore well constrain the nature of their mantle source (Sobolev *et al.* 2007; Herzberg, 2011; Foley *et al.* 2013; Herzberg et al. 2016). Experimental studies show that the olivine crystallized from melts derived from pyroxenite have 100×Mn/Fe values of 1.05–1.35, whereas those in melts derived from peridotite source show higher 100×Mn/Fe values (>1.5) (Sobolev *et al.* 2007; Foley *et al.* 2013). The Dali picrites have olivine phenocrysts with higher Mn content compared with those of Karoo or Hawaii, and show a similar trend to the Mn content of MORB (Fig. 4). Additionally, the high 100×Mn/Fe ratios (1.43–1.73) of olivine in Dali picrites are consistent with those olivines crystallized from melts derived from peridotite (Fig. 5b). This evidence indicates that the primary magma of the Dali picrites was more likely derived from a peridotite-dominated source.

Sobolev *et al.* (2007) suggested that the percentage of metasomatic pyroxenite (X_{px}) in the mantle source could be calculated based on the Mn/Fe values of the olivine phenocrysts. The equation was proposed as: $X_{px} = 3.48−[2.071×(100×Mn/Fe)]$. Combined with the trace-element data from LA-ICP-MS analysis (online Supplementary Table S2), we calculate an average X_{px} in the Dali picrite mantle source of 22.6% (Fig. 6). For comparison, Sobolev *et al.* (2007) suggested an average X_{px} value of 17% for MORBs. However, the data for olivine in MORB reported by these
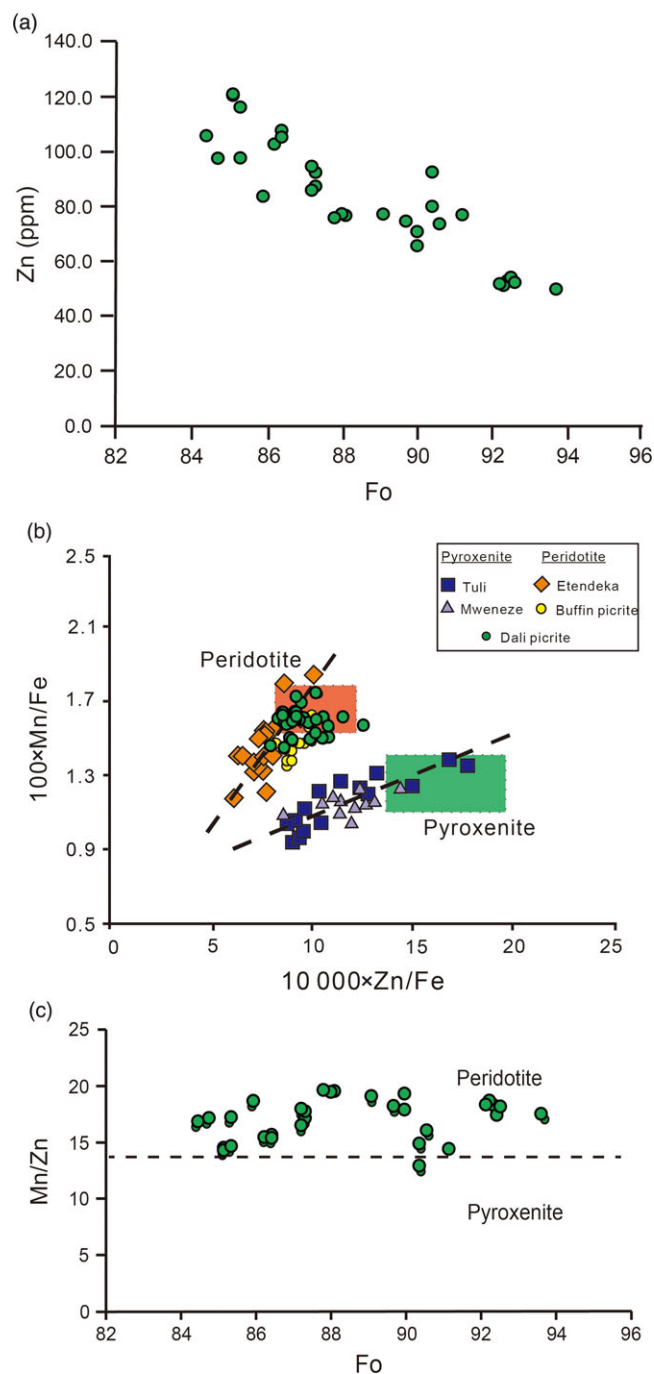

Fig. 5. (Colour online) (a) Diagram of Zn concentrations versus forsterite (Fo) values of olivine phenocrysts in Dali picrites. (b) 100×Mn/Fe versus 10 000×Zn/Fe of primitive olivines in the Dali picrites. Tuli, Mwenezi, Etendeka and Buffin picrite data from Howarth & Harris (2017). (c) Mn/Zn ratio of the olivine phenocrysts. Olivine from a pyroxenite-derived melt is characterized by low Mn/Zn ratios (<14), while those from peridorite-derived melt have high ratios (>14).

authors spans a somewhat larger range in X_{px} values, which show a similar range to the Dali picrites (Fig. 6); this suggests that the mantle source of Dali picrites is not pyroxenite dominated. It is notable that high pressure may increase the partitioning of Mn between olivine and melts ($K_D Mn^{ol/melt}$) (Matzen *et al.* 2017). Our calculation of X_{px} using the method of Sobolev *et al.* (2007) is therefore very likely to be flawed.
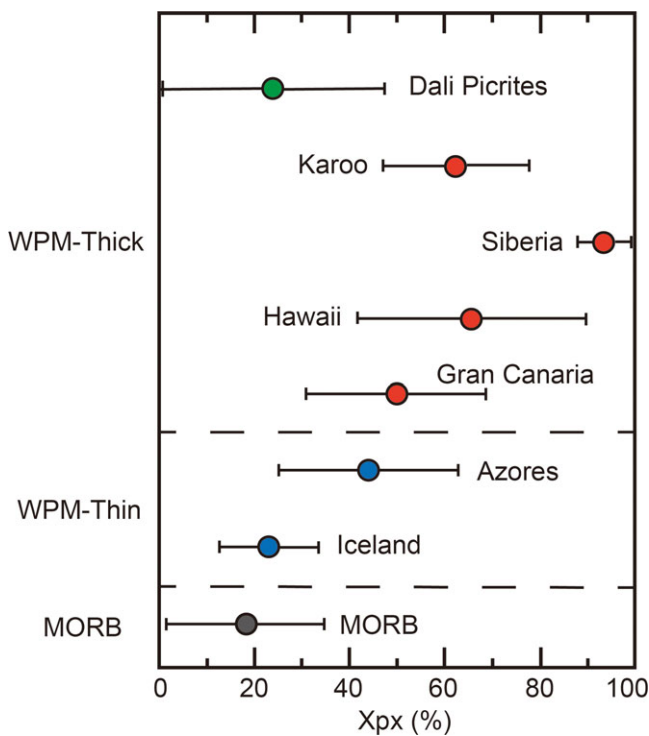
Fig. 6. (Colour online) The percentage of pyroxenite in the mantle source (Xpx) calculated based on Mn/Fe ratios of olivine phenocrysts in Dali picrites and picrites and basalts from Siberian large igneous province (LIP), Hawaii, Karoo LIP, Gran Canaria, Azores, Iceland and MORBs (Sobolev *et al.* 2007).

The ratio of inter-mineral exchange coefficient of Zn/Mn between olivine and clinopyroxene, $K_D(Zn/Mn)^{cpx/ol}$, defined as $K_D(Zn/Mn)^{cpx/melt}/K_D(Zn/Mn)^{ol/melt}$, is *c.* 0.26 (Le Roux *et al.* 2010). It has also been established that $K_D(Zn/Fe)^{ol/melt}$ is close to 1, but for clinopyroxene $(K_D(Zn/Fe)^{cpx/melt})$, the value is much lower (Le Roux *et al.* 2010). This suggests that Zn/Fe is minimally fractionated during partial melting of peridotite mantle, but strongly fractionated during melting of pyroxene. As demonstrated previously, olivine grains in magmas derived from peridotite-dominated sources and pyroxenite-dominated sources have significantly different variation trends when plotted in the 100×Mn/Fe versus 10 000×Zn/Fe diagram (Howarth & Harris, 2017). Moreover, olivine equilibrated with melts derived from pyroxenite was demonstrated to have 10 000×Zn/Fe values of >14 (Le Roux *et al.* 2010; Howarth & Harris, 2017). Olivines in Dali picrites have 10 000×Zn/Fe values of 8.0–12.7, showing a similar trend to olivine in picrites from Edenteka and Baffin Island, which were derived from a peridotite source (Fig. 5b). In addition, olivine crystallized from pyroxenite-derived melts have a relatively low Mn/Zn ratio (<14), while those from peridotite-derived melts exhibit a higher Mn/Zn ratio (>14). The Mn/Zn values of the olivine in the Dali picrite range from 13.6 to 18.4, with most Mn/Zn values >15, also indicating a peridotite dominate source (Fig. 5c).

All the features presented above suggest that Dali picrites are more likely to have formed from peridotite-dominated mantle source. However, how a peridotite source can produce a picrite with high-Ni olivine phenocrysts needs to be evaluated further. According to recent experimental studies, the partition coefficient of the Ni element between olivine and melts ($K_D Ni^{ol/melt}$) is mainly controlled by temperature and pressure. Under conditions of high temperature and pressure, the Ni partition coefficient ($K_D Ni^{ol/melt}$)

will decrease and result in less Ni left in residual olivine. As the melts rise to a shallower level or even to the sub-surface, the partition coefficient of Ni between olivine and melts ($K_D Ni^{ol/melt}$) will increase due to the decreasing pressure. This may result in higher Ni concentrations in olivine phenocrysts, which are even higher than those in residual olivine in mantle (Li & Ripley, 2010; Niu *et al.* 2011; Matzen *et al.* 2013, 2017).

Matzen *et al.* (2013) presented results from experimental work which allowed them to investigate the effects of temperature (*T*) and pressure (*P*) on $K_D Ni^{ol/melt}$, independent of substantial changes in liquid composition. The partition coefficient of Ni between olivine and melts is described by the equation:

$$\ln\left(K_D Ni^{ol/liq}\right) = \left[(-\Delta_r H_{Tref,\,Pref})/(RT)\right] + (\Delta_r S^o{}_{Tref,\,Pref}/R)$$
$$- \ln[X(MgO)^{liq}/X(MgSi_{0.5}O_2)^{ol}]$$

where $-\Delta_r H_{Tref,\,Pref}/R$ and $\Delta_r S^o{}_{Tref,\,Pref}/R$ are constants independent of pressure and temperature, and *T* is the olivine liquidus temperature in degrees Kelvin. Putirka *et al.* (2018) reproduced the calibration data ($n = 17$) with a standard error of estimate of ± 1.3 with an R^2 of 0.82, using the high-precision work of Matzen *et al.* (2013). The above equation can be simplified to:

$$K_D Ni^{ol/lir} = e^{(3349/T)-0.79}$$

where the olivine liquidus temperature *T* is in degrees Celsius. From a rough estimate of the source region pressure via the inversion of lanthanide REE data and olivine–melt equilibrium, the pressure at the start of melting is estimated as 4 GPa (Xu *et al.* 2001; Zhang *et al.* 2003, 2006). Tao *et al.* (2015) used the olivine and clinopyroxene composition in ELIP picrites to determine the *P-T* condition when magma crystallization occurred, and reported that the olivine phenocrysts crystallized at a pressure of 1 GPa. As we calculate later in Section 5.b, the olivines in Dali picrites crystallized at a temperature of *c.* 1491°C, and the mantle potential temperature T_p is *c.* 1560°C. When these temperature estimates are introduced into the simplified equation above, the resulting Ni partition coefficient $K_D Ni^{ol/melt}$ is *c.* 3.8 and 4.3 for melting and crystallizing, respectively. The Ni content of melts derived from peridotite is defined as:

$$Ni_{melt} = 2.9594 \times MgO_{melt}^{1.859}$$

where Ni is in ppm and MgO in wt%, provided by Niu *et al.* (2011).

According to the olivine–bulk-rock equilibrium and melt inclusions data, previous studies suggested that the primary melt of the Dali picrites had MgO content of 20–23 wt% (Li *et al.* 2012, 2014; Ren *et al.* 2017). When we use the primary melt MgO content in the equation above, the Ni content is 776–1006 ppm. The Dali picrites melted at high pressure (*c.* 4 GPa), adiabatically ascended to the near-surface environment at low pressure (*c.* 1 GPa) and started to crystallize olivine. In this case, the Ni partition coefficient $K_D Ni^{ol/melt} = 4.3$. In order to crystallize olivine with *c.* 3900 ppm Ni concentration, there should be at least *c.* 907 ppm Ni in the melt. This is consistent with the calculated Ni concentration in the primary melt of Dali picrite, suggesting that it is possible for the Dali picrite melt to crystallize high-Ni olivines. In other words, the Dali picrites were produced by partial melting of a peridotite source. We therefore propose that the high concentration of Ni in olivine in the Dali picrites might be attributed to the relatively low $K_D Ni^{ol/melt}$ during peridotite partial melting at conditions of high temperature
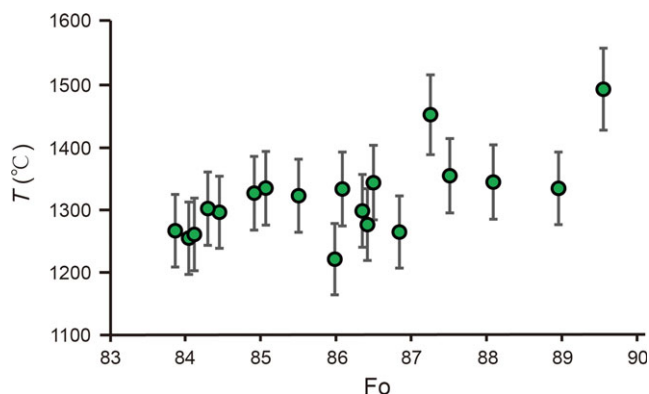
Fig. 7. (Colour online) Results of Al-in-olivine thermometry for the Dali picrites shown in olivine Fo versus T (°C). Estimated 2σ errors for the temperatures are shown (see Section 5.b).

Table 1. The highest-reported olivine–spinel equilibrium temperature and the Fo values for the host olivines. Data sources: MORB, Gorgona, SE Greenland, Baffin Island and Madagascar: Coogan *et al.* (2014); Karoo: Heinonen *et al.* (2015); Etendeka: Jennings *et al.* (2019); ELIP: Xu & Liu (2016); Iceland: Matthews *et al.* (2016).

Type	Province	Fo	T (°C)
MORB	–	89	1270
Iceland	–	90.7	1399
LIP	ELIP (Dali picrites in this study)	89.4	1491
	ELIP (reported by Xu & Liu, 2016)	88.3	1440
	Karoo	91.7	1481
	Etendeka	92.9	1511
	Madagascar	91.8	1485
	Gorgona	91.7	1434
	SE Greenland	89.8	1353
	Baffin Island	90.8	1408

and high pressure, which resulted in enrichment of the primitive magmas with Ni, and the high $K_D Ni^{ol/melt}$ when the deep mantle-derived magma rose to a shallower environment of lower temperature and pressure, which resulted in crystallization of those Ni-rich olivines. There is therefore no need for eclogites or pyroxenite in the generation of Dali picrites.

5.b. Estimation of mantle potential temperature

Based on the temperature-dependent behaviour of Al between coexisting olivine and Cr-spinel, the newly established Al-in-olivine thermometer proposed by Wan *et al.* (2008) and Coogan *et al.* (2014) can be used to estimate the olivine crystallization temperature. Compared with the traditional olivine–melt equilibrium thermometer, Al-in-olivine thermometer has the advantage of being independent of crystallization pressure, parental melt composition, oxygen fugacity and water content (Wan *et al.* 2008; Coogan *et al.* 2014). In addition, Al is expected to diffuse much more slowly through the olivine lattice than Mg and Fe, so the initial composition of the olivine-spinel pair is preserved (Spandler & O'Neill, 2010). It is therefore much more useful and convenient for us to determine the crystallization temperature of olivines in Dali picrites. The experimental results provided by Wan *et al.* (2008) and Coogan *et al.* (2014) suggested a restricted range for this thermometer; only Cr-spinel with Cr no. of 0–0.69 (Cr/(Cr + Al), mol) can be used for a reliable result from the Al-in-ol thermometer. The spinels in this study exhibit Cr no. values in the range of 0.570–0.685, all within the calibration range of the thermometer. We can therefore use these olivine and Cr-spinel composition data to estimate the crystallization temperature of olivines (°C), and the thermometer calibration equation is expressed:

$$T^{ol-spl} = 273.15 + 10\,000/[0.575 + (0.884 \times \text{Cr no.}) - 0.897 \times \ln(Al_2O_3^{ol}/Al_2O_3^{sp})].$$

The calculated temperature for Dali picrites ranges from 1221 to 1491°C (by EPMA data, online Supplementary Table S1c). Accordingly, we also calculated the uncertainty of the thermometer by error propagation, and the calculated 2σ error ranged from ± 57 to ± 65°C (online Supplementary Table S1c). The maximum crystallization temperature is estimated as 1491 ± 65°C (Fig. 7), which constrains the liquidus temperature to $T^{ol/liq} \geq 1491°C$. When compared with olivine crystallization temperatures reported from

other plume-related settings, such as continental flood basalts or other LIPs, the hottest Dali olivine–spinel crystallization temperatures are *c.* 50°C higher than the maximum olivine crystallization temperatures for ELIP samples from Yongsheng, Binchuan and Dali estimated by Xu & Liu (2016) (1440 ± 63°C). The samples of Dali picrite for this study were collected from a road-cut section located close to the Dali sections where Xu & Liu (2016) collected their samples, and the higher crystallization temperature estimated in Dali picrites might be attributed to their higher Fo value of the host olivine than the samples of Xu & Liu (2016). For comparison, the highest Dali picrite olivine crystallization temperature is 1491°C, which is similar to the highest olivine crystallization temperature estimated for Karoo, Madagascar and Etendeka, but about 100°C higher than those estimated for Iceland and SE Greenland (Coogan *et al.* 2014; Heinonen *et al.* 2015; Xu & Liu, 2016; Matthews *et al.* 2016; Jennings *et al.* 2019; Table 1). This temperature is about 200°C higher than the maximum crystallization temperature of MORB (1270°C) calculated by the same thermometer (Coogan *et al.* 2014), and provides robust evidence for a pronounced thermal anomaly in the mantle source of the Dali picrites.

As for the mantle potential temperature (T_P), there is a simple method for evaluating T_P of a peridotite source from the olivine crystallization temperature. It is generally considered that progressively ascending melts are nearly adiabatic before olivine begins to crystallize. Because of the enthalpy of melting and adiabatic cooling, T_P should be higher than the maximum crystallization temperature. In order to calculate T_P of the Dali picrites, a temperature correction for melt generation and adiabatic cooling is required (Putirka *et al.* 2007; Herzberg & Asimow, 2015; Matthews *et al.* 2016; Jennings *et al.* 2019). Putirka *et al.* (2007) and Herzberg & Asimow (2015) assumed a simple two-step approach to calculate the mantle potential temperature from the crystallization temperature: first, correct back to the liquidus temperature at 1 atm along an adiabat, then correct the temperature which dropped through melting and crystallizing at 1 atm.

The water content of magma also needs to be taken into consideration, due to its potential effect on the T_P calculation. As reported by Liu *et al.* (2017), the H_2O contents in Dali picrites were calculated to be 2–4 wt% based on the study on

clinopyroxene–melt equilibrium. However, considering that the crystallization of olivine and spinel usually occurs earlier than that of clinopyroxene, an increase of H_2O in the residual melts can be expected, and the reported H_2O contents might be an overestimate. As our samples lack other hydrous primary minerals (e.g. amphibole, mica) and the basalts coexisting with Dali picrites (Fig. 2a) contain large amounts of plagioclase phenocrysts (Fig. 2d), we propose that the water content of our Dali pictrite samples was probably relatively low.

Based on experimental data, Herzberg & Asimow (2015) defined the effect of pressure on increasing olivine liquidus temperature as:

$$T_1^{ol/lig} = T(P)^{ol/liq} - 54P + 2P^2$$

where $T_1^{ol/liq}$ (°C) is the olivine liquidus temperature at a pressure of 1 atm and $T(P)^{ol/liq}$ (°C) is the olivine liquidus temperature at pressure P in gigapascals. Tao *et al.* (2015) suggested that the olivine crystallization pressure is *c.* 1 GPa, and the liquidus temperature $T(P)^{ol/liq}$ is constrained to ≥1491°C, resulting in $T_1^{ol/liq} \geq 1439$°C. The mantle potential temperature T_P is related to the olivine liquid temperature at 1 atm ($T_1^{ol/liq}$) along the solidus line by the equation (Herzberg & Asimow, 2015):

$$T_p = 1.049 \times T_1^{ol/liq} - [0.00019 \times (T_1^{ol/liq})^2]$$
$$+ [1.487 \times 10^{-7} \times (T_1^{ol/liq})^3].$$

Using $T_1^{ol/liq}$ in the above equation, we obtain a T_P of 1559°C. We also consider the uncertainty of the crystallization temperature in the calculation, yielding a propagated uncertainty in T_P of *c.* +95/–90°C. We therefore infer that the mantle potential temperature of the Dali picrites is ≥ 1559 +95/–90°C, which is consistent with previous studies (*c.* 1620°C; Zhang *et al.* 2006). For comparison, Matthews *et al.* (2016) used a similar method to calculate a T_P of 1480 +37/–30°C for the Iceland mantle plume and 1318 +44/–32°C for the MORB from the olivine–spinel crystallization temperatures. The mantle potential temperature of the Dali picrites is *c.* 200°C higher than that of normal MORB, and is therefore consistent with a plume-head origin (even if our method represents a simplification and neglects the uncertainty in water content, oxygen fugacity and the melt fractions). The mantle potential temperature T_P is definitely higher than the olivine crystallization temperature, and $T^{ol–spl} = 1491$°C is still much higher than the mantle potential temperature of the normal MORB $T_P(MORB) = 1318$ +44/–32°C).

6. Conclusions

1. The trace-element data of primitive olivine in Dali picrites are consistent with a peridotite-dominated source for the primary magma.
2. The high Ni content in olivine phenocrysts can be explained by the relatively low $K_DNi^{ol/melt}$ during partial melting in the deep mantle and the high $K_DNi^{ol/melt}$ during crystallization in the relatively shallow level. This model suggests that a significant contribution from a metasomatic pyroxenite to the formation of high-Ni olivine is not a prerequisite.
3. Based on the Al-in-olivine thermometer, we compute the maximum olivine crystallization temperature $T^{ol–spl}$ of 1491 ± 65°C. Since the Dali picrite was derived from a peridotite-dominated source, the estimated mantle potential temperature T_P is ≥ 1559

+95/–90°C, which is *c.* 200°C higher than the mantle potential temperature of the MORB, confirming the role of a mantle plume.

References

Ali JR, Fitton JG and Herzberg C (2010) Emeishan large igneous province (SW China) and the mantle-plume up-doming hypothesis. *Journal of the Geological Society* **167**, 953–59.

Ali JR, Thompson GM, Zhou MF and Song XY (2005) Emeishan large igneous province, SW China. *Lithos* **79**, 475–89.

Campbell IH (2005) Large igneous provinces and the mantle plume hypothesis. *Elements* **1**, 265–69.

Campbell IH (2007) Testing the plume theory. *Chemical Geology* **241**, 153–76.

Campbell IH and Griffins RW (1990) Implications of mantle plume structure for the evolution of flood basalts. *Earth and Planetary Science Letters* **99**, 79–93.

Chen L, Zhi XC, Zhang ZC and Shim RD (2007) Preliminary study on Re-Os isotope geochemistry of picrites from Lijiang Area, Yunnan Province. *Geological Journal of China Universities* **13**, 337–43 (in Chinese with English abstract).

Chung SL and Jahn BM (1995) Plume-lithosphere interaction in generation of the Emeishan flood basalts at the Permian–Triassic boundary. *Geology* **23**, 889–92.

Condie KC and Puetz SJ (2019) Time series analysis of mantle cycles Part II: the geologic record in zircons, large igneous provinces and mantle lithosphere. *Geoscience Frontiers* **10**, 1327–36.

Coogan LA, Saunders AD and Wilson RN (2014) Aluminum-in-olivine thermometry of primitive basalts: evidence of an anomalously hot mantle source for large igneous provinces. *Chemical Geology* **368**, 1–10.

De Hoog JCM, Gall L and Cornell DH (2010) Trace-element geochemistry of mantle olivine and application to mantle petrogenesis and geothermobarometry. *Chemical Geology* **270**, 196–215.

Foley SF, Jacob DE and O'Neill HSC (2011) Trace element variations in olivine phenocrysts from Ugandan potassic rocks as clues to the chemical characteristics of parental magmas. *Contributions to Mineralogy and Petrology* **162**, 1–20.

Foley SF, Prelevic D, Rehfeldt T and Jacob DE (2013) Minor and trace elements in olivines as probes into early igneous and mantle melting processes. *Earth and Planetary Science Letters* **363**, 181–91.

Hanski E, Kamenetsky VS, Luo ZY, Xu YG and Kuzmin DV (2010) Primitive magmas in the Emeishan Large Igneous Province, southwestern China and northern Vietnam. *Lithos* **119**, 75–90.

Hanski E, Walker RJ, Huhma H, Polyakov GV, Balykin PA, Trong HT and Thi PN (2004) Origin of the Perm-Triassic komatiites, northwestern Vietnam. *Contributions to Mineralogy and Petrology* **147**, 453–69.

Hao YL, Huang QS, Zhang XR and Shi RD (2011) Re-Os isotopes of Dali picrite (Yunnan): new constraints on the formation of Emeishan Large Igneous Province. *Acta Petrologica Sinica* **27**, 2937–46 (in Chinese with English abstract).

He B, Xu YG, Chung SL, Xiao L and Wang Y (2003) Sedimentary evidence for a rapid, kilometer-scale crustal doming prior to the eruption of the Emeishan flood basalts. *Earth and Planetary Science Letters* **213**, 391–405.

He B, Xu YG, Huang XL, Luo ZY, Shi YR, Yang QJ and Yu SY (2007) Age and duration of the Emeishan flood volcanism, SW China: Geochemistry and SHRIMP zircon U-Pb dating of silicic ignimbrites, post-volcanic Xuanwei

Formation and clay tuff at the Chaotian section. *Earth and Planetary Science Letters* 255, 306–23.

Heinonen JS, Jennings ES and Riley TR (2015) Crystallisation temperatures of the most Mg-rich magmas of the Karoo LIP on the basis of Al-in-olivine thermometry. *Chemical Geology* 411, 26–35.

Herzberg C (2006) Petrology and thermal structure of the Hawaiian plume from Mauna Kea volcano. *Nature* 444, 605–09.

Herzberg C (2011) Identification of source lithology in the Hawaiian and Canary Islands: implications for origins. *Journal of Petrology* 52, 113–46.

Herzberg C and Asimow PD (2015) PRIMELT3 MEGA.XLSM software for primary magma calculation: peridotite primary magma MgO contents from the liquidus to the solidus. *Geochemistry, Geophysics, Geosystems* 16, 563–78.

Herzberg C, Asimow PD, Ionov DA, Vidito C, Jackson MG and Geist D (2013) Nickel and helium evidence for melt above the core–mantle boundary. *Nature* 493, 393–97.

Herzberg C, Vidito C and Starkey NA (2016) Nickel-cobalt contents of olivine record origins of mantle peridotite and related rocks. *American Mineralogist* 101, 1952–66.

Howarth GH and Harris C (2017) Discriminating between pyroxenite and peridotite sources for continental flood basalts (CFB) in southern Africa using olivine chemistry. *Earth and Planetary Science Letters* 475, 143–51.

Humayun M, Qin LP and Norman MC (2004) Geochemical evidence for excess iron in the mantle beneath Hawaii. *Science* 306, 91–94.

Ionov DA (2007) Compositional variations and heterogeneity in fertile lithospheric mantle: peridotite xenoliths in basalts from Tariat, Mongolia. *Contributions to Mineralogy and Petrology* 154, 455–77.

Jennings ES, Gibson SA and MacLennan J (2019) Hot primary melts and mantle source for the Paraná-Etendeka flood basalt province: new constraints from Al-in-olivine thermometry. *Chemical Geology* 529, 119287.

Jerram DA, Widdowson M, Wignall PB, Sun YD, Lai XL, Bond DP and Torsvik TH (2016) Submarine paleoenvironments during Emeishan flood basalt volcanism, SW China: implications for plume–lithosphere interaction during the Capitanian, middle Permian ('end Guadalupian') extinction event. *Palaeogeography, Palaeoclimatology, Palaeoecology* 441, 65–73.

Kamenetsky VS, Chung SL, Kamenetsky MB and Kuzmin DV (2012) Picrites from the Emeishan large igneous province, SW China: a compositional continuum in primitive magmas and their respective mantle sources. *Journal of Petrology* 53, 2095–113.

Le Roux V, Lee CT and Turner SJ (2010) Zn/Fe systematics in mafic and ultramafic systems: implications for detecting major element heterogeneities in the Earth's mantle. *Geochimica et Cosmochimica Acta* 74, 2779–96.

Li C and Ripley EM (2010) The relative effects of composition and temperature on olivine-liquid Ni partitioning: statistical deconvolution and implications for petrologic modeling. *Chemical Geology* 275, 99–104.

Li HB, Zhang ZC, Ernst R, Lu LS, Santosh M, Zhang DY and Cheng ZG (2015) Giant radiating mafic dyke swarm of the Emeishan large igneous province, identifying the mantle plume centre. *Terra Nova* 27, 247–57.

Li J, Wang XC, Ren ZY, Xu JF, He B and Xu YG (2014) Chemical heterogeneity of the Emeishan mantle plume: evidence from highly siderophile element abundances in picrites. *Journal of Asian Earth Sciences* 79, 191–205.

Li J, Xu JF, Suzuki K, He B, Xu YG and Ren ZY (2010) Os, Nd, Sr isotope and trace element geochemistry of the Muli picrites: insights into the mantle source of the Emeishan large igneous province. *Lithos* 119, 108–22.

Li YS, Zhang ZC and Nie BF (2012) An improved simple method for estimating primitive magma – a case for the picrites in the Lijiang area of Emeishan large igneous province. *Geological Review* 4, 653–59 (in Chinese with English abstract).

Liu J, Xia QK, Kuritani T, Hanski E and Yu HR (2017) Mantle hydration and the role of water in the generation of large igneous provinces. *Nature Communications* 8, 1–7.

Liu Y, Hu Z, Gao S, Günther D, Xu J, Gao C and Chen H (2008) In situ analysis of major and trace elements of anhydrous minerals by LAICP-MS without applying an internal standard. *Chemical Geology* 257, 34–43.

Matthews S, Shorttle O and MacLennan J (2016) The temperature of the Icelandic mantle from olivine-spinel aluminum exchange thermometry. *Geochemistry, Geophysics, Geosystems* 17, 4725–52.

Matzen AK, Baker MB, Beckett JR and Stolper EM (2013) The temperature and pressure dependence of nickel partitioning between olivine and silicate melt. *Journal of Petrology* 54, 2521–45.

Matzen AK, Wood BJ, Baker MB and Stolper EM (2017) The roles of pyroxenite and peridotite in the mantle sources of oceanic basalts. *Nature Geoscience* 10, 530–35.

McDonough WF and Sun SS (1995) The composition of the Earth. *Chemical Geology* 120, 223–53.

Ning SY, Wang FY, Xue WD and Zhou TF (2017) Geochemistry of the Baoshan pluton in the Tongling region of the Lower Yangtze River Belt. *Geochimica* 46, 397–412 (in Chinese with English abstract).

Niu YL, Wilson M, Humphreys ER and O'Hara MJ (2011) The origin of intraplate ocean island basalts (OIB): the lid effect and its geodynamic implications. *Journal of Petrology* 52, 1443–68.

Peate IU, Bryan SE, Wignall PB, Jerram DA and Ali JR (2011) Comment on 'Paleokarst on the top of the Maokou Formation: further evidence for domal crustal uplift prior to the Emeishan flood volcanism'. *Lithos* 119, 1–9.

Putirka KD, Perfit M, Ryerson FJ and Jackson MG (2007) Ambient and excess mantle temperatures, olivine thermometry, and active vs. passive upwelling, *Chemical Geology* 241, 177–206.

Putirka K, Ryerson FJ, Perfit M and Ridley WI (2011) Mineralogy and composition of the oceanic mantle. *Journal of Petrology* 52, 279–313.

Putirka K, Tao Y, Hari KR, Perfit MR, Jackson MG and Arevalo R (2018) The mantle source of thermal plumes: trace and minor elements in olivine and major oxides of primitive liquids (and why the olivine compositions don't matter). *American Mineralogist* 103, 1253–70.

Ren ZY, Wu YD, Zhang L, Nichols AR, Hong LB, Zhang YH, Zhang Y, Liu JQ and Xu YG (2017) Primary magmas and mantle sources of Emeishan basalts constrained from major element, trace element and Pb isotope compositions of olivine-hosted melt inclusions. *Geochimica et Cosmochimica Acta* 208, 63–85.

Richards MA, Duncan RA and Courtillot VE (1989) Flood basalts and hotspot tracks: plume heads and tails. *Science* 246, 103–107.

Santosh M, Hari KR, He XF, Han YS and Manu Prasanth MP (2018) Oldest lamproites from Peninsular India track the onset of Paleoproterozoic plume-induced rifting and the birth of large igneous province. *Gondwana Research* 55, 1–20.

Shellnutt JG (2014) The Emeishan large igneous province: a synthesis. *Geoscience Frontiers* 5, 369–94.

Shellnutt JG, Denyszyn S and Mundil R (2012) Precise age determination of mafic and felsic intrusive rocks from the Permian Emeishan large igneous province (SW China). *Gondwana Research* 22, 118–26

Shellnutt JG and Pham TT (2018) Mantle potential temperature estimates and primary melt compositions of the low-Ti Emeishan flood basalt. *Frontiers in Earth Science* 6, 1–10.

Shellnutt JG, Zhou MF, Yan DP and Wang YB (2008) Longevity of the Permian Emeishan mantle plume (SW China): 1 Ma, 8 Ma or 18 Ma? *Geological Magazine* 145, 373–88.

Sobolev AV, Hofmann AW, Kuzmin DV, Yaxley GM, Arndt NT, Chung SL, Danyushevsky LV, Elliott T, Frey FA and Garcia MO (2007) The amount of recycled crust in sources of mantle-derived melts. *Science* 316, 412–17.

Sobolev AV, Hofmann AW, Sobolev SV and Nikogosian IK (2005) An olivine-free mantle source of Hawaiian shield basalts. *Nature* 434, 590–97.

Song XY, Zhou MF, Cao ZM and Robinson PT (2004) Late Permian rifting of the South China Craton caused by the Emeishan mantle plume? *Journal of the Geological Society* 161, 773–81.

Song XY, Zhou MF, Hou ZQ, Cao ZM, Wang YL and Li Y (2001) Geochemical constraints on the mantle source of the Upper Permian Emeishan continental flood basalts, southwestern China. *International Geology Review* 43, 213–25.

Spandler C and O'Neill HSC (2010) Diffusion and partition coefficients of minor and trace elements in San Carlos olivine at 1,300 °C with some geochemical implications. *Contributions to Mineralogy and Petrology* 159, 791–818.

Starkey NA, Stuart FM, Ellam RM, Fitton JG, Basu S and Larsen LM (2009) Helium isotopes in early Iceland plume picrites: constraints on the composition of high ^{3}He/^{4}He mantle. *Earth and Planetary Science Letters* 277, 91–100.

Sun YD, Lai XL and Wignall PB (2010) Dating the onset and nature of the Middle Permian Emeishan large igneous province eruptions in SW China using conodont biostratigraphy and its bearing on mantle plume uplift models. *Lithos* **119**, 20–33.

Tao Y, Putirka K, Hu RZ and Li C (2015) The magma plumbing system of the Emeishan large igneous province and its role in basaltic magma differentiation in a continental setting. *American Mineralogist* **100**, 2509–17.

Wan Z, Coogan LA and Canil D (2008) Experimental calibration of aluminum partitioning between olivine and spinel as a geothermometer. *American Mineralogist* **93**, 1142–47.

Wang CY, Ge C, Ning SY, Nie LQ, Zhong GX and White N (2017) A new approach to LA-ICP-MS mapping and application in geology. *Acta Petrologica Sinica* **33**, 3422–36 (in Chinese with English abstract).

Wu YD, Ren ZY, Handler MR, Zhang L, Qian SP, Xu YG, Wang CY, Wang Y and Chen LL (2018) Melt diversity and magmatic evolution in the Dali Picrites, Emeishan Large Igneous Province. *Journal of Geophysical Research: Solid Earth* **123**, 9635–57.

Xiao L, Xu YG, Chung SL, He B and Mei HJ (2003) Chemostratigraphic correlation of Upper Permian lavas from Yunnan province, China: extent of the Emeishan Large Igneous Province. *International Geology Review* **45**, 753–66.

Xiao L, Xu YG, Mei HJ, Zheng YF, He B and Pirajno F (2004) Distinct mantle sources of low-Ti and high-Ti basalts from the western Emeishan large igneous province, SW China: implications for plume–lithosphere interaction. *Earth and Planetary Science Letters* **228**, 525–46.

Xu JF, Suzuki K, Xu YG, Mei HJ and Li J (2007) Os, Pb, and Nd isotope geochemistry of the Permian Emeishan continental flood basalts: insights into the source of a large igneous province. *Geochimica et Cosmochimica Acta* **71**, 2104–19.

Xu R and Liu Y (2016) Al-in-olivine thermometry evidence for the mantle plume origin of the Emeishan large igneous province. *Lithos* **266–267**, 362–66.

Xu YG, Chung SL, Jahn BM and Wu G (2001) Petrologic and geochemical constraints on the petrogenesis of Permian-Triassic Emeishan flood basalts in southwestern China. *Lithos* **58**, 145–68.

Xu YG, Chung SL, Shao H and He B (2010) Silicic magmas form the Emeishan large igneous province, southwest China: petrogenesis and their link with the end-Guadalupian biological crisis. *Lithos* **119**, 47–60.

Xu YG, He B, Chung SL, Menzies MA and Frey FA (2004) Geologic, geochemical, and geophysical consequences of plume involvement in the Emeishan flood-basalt province. *Geology* **32**, 917–20.

Yao JH, Zhu WG, Li C, Zhong H, Yu SY, Ripley EM and Bai ZJ (2019) Olivine O isotope and trace element constraints on source variation of picrites in the Emeishan flood basalt province, SW China. *Lithos* **338–339**, 87–98.

Yu SY, Shen NP, Song XY, Ripley EM, Li C and Chen LM (2017) An integrated chemical and oxygen isotopic study of primitive olivine grains in picrites from the Emeishan large Igneous Province, SW China: evidence for oxygen isotope heterogeneity in mantle sources. *Geochimica et Cosmochimica Acta* **215**, 263–276.

Yu SY, Song XY, Chen LM and Li XB (2014) Postdated melting of subcontinental lithospheric mantle by the Emeishan mantle plume: evidence from the Anyi intrusion, Yunnan, SW China. *Ore Geology Reviews* **57**, 560–73.

Zhang ZC, Hao YL and Wang FS (2003) Picrites in large igneous provinces and their implications. *Earth Science Frontiers* **10**, 105–14.

Zhang ZC, Hao YL, Wang FS and Mahoney JJ (2004) Petrology, mineralogy and geochemistry of the Emeishan continental flood basalts, SW China: evidence for activity of mantle plumes. *Acta Geological Sinica* **78**, 40–51.

Zhang ZC, Mahoney JJ, Mao J and Wang F (2006) Geochemistry of picritic and associated basalt flows of the western Emeishan flood basalt province, China. *Journal of Petrology* **47**, 1997–2019.

Zhang ZC, Zhi XC, Chen L, Saunder AD and Reichow M (2008) Re-Os isotopic compositions of picrites from the Emeishan flood basalt province, China. *Earth and Planetary Science Letters* **276**, 30–39.

Zhong H, Campbell IH, Zhu WG, Allen CM, Hu RZ, Xie LW and He DF (2011) Timing and source constraints on the relationship between mafic and felsic intrusions in the Emeishan large igneous province. *Geochimica et Cosmochimica Acta* **75**, 1374–95.

Zhong H, Zhu WG, Hu RZ, Xie LW, He DF, Liu F and Chu ZY (2009) Zircon U–Pb age and Sr–Nd–Hf isotope geochemistry of the Panzhihua A-type syenitic intrusion in the Emeishan large igneous province, southwest China and implications for growth of juvenile crust. *Lithos* **110**, 109–28.

Zhong YT, He B, Mundil R and Xu YG (2014) CA-TIMS zircon U-Pb dating of felsic ignimbrite from the Binchuan section: implications for the termination age of Emeishan large igneous province. *Lithos* **204**, 14–19.

Zhou MF, Yan DP, Kennedy AK, Li Y and Ding J (2002) SHRIMP U–Pb zircon geochronological and geochemical evidence for Neoproterozoic arc-magmatism along the western margin of the Yangtze Block, South China. *Earth and Planetary Science Letters* **196**, 51–67.

Zhu J, Zhang ZC, Reichow MK, Li HB, Cai WC and Pan RH (2018) Weak vertical surface movement caused by the ascent of the Emeishan mantle anomaly. *Journal of Geophysical Research: Solid Earth* **123**, 1–17.